Journal of the European Ceramic Society **12** (1993) 15–25

Ultrasonic Imaging and Characterisation of Surface Breaking Cracks in Silicon Nitride by Leaky Rayleigh Waves

P. Lemaitre,[a] V. Buglino,[b] F. Lakestani[a] & R. Denis[a]

[a] Commission of the European Communities, Joint Research Centre, Institute for Advanced Materials, Non-Destructive Evaluation Unit, TP 750, I-21020 Ispra, Italy

[b] Universtà degli Studi di Palermo, Dipartimento di Meccanica ed Aeronautica, Viale delle Scienze, I-90128 Palermo, Italy

(Received 26 June 1992; revised version received 25 November 1992; accepted 7 December 1992)

Abstract

The detection, imaging and characterisation of radial cracks, resulting from Vickers indentations in a sintered reaction-bonded silicon nitride, are studied by means of ultrasonic leaky Rayleigh waves. The depth of the cracks investigated varied between 40 and 270 μm. Focusing probes with a nominal frequency of 30 and 75 MHz are used. The obtained C-scan images, which are complicated by the presence of the indents, are discussed. Crack length and crack depth are measured using acoustic methods. The detection and sizing limits are discussed.

Die Identifizierung, Abbildung und Charakterisierung von radialen Rissen, die durch Vickers Härteindrücke in reaktionsgesintertem Siliziumnitrid erzeugt wurden, werden mit Hilfe von Rayleigh wellen untersucht. Die untersuchten Rißtiefen liegen zwischen 40 und 270 μm. Es werden Sonden mit Nominalfrequenzen von 30 MHz und 75 MHz benutzt. Die erhaltenen C-scan Abbildungen, die durch die vorhandenen Eindrücke beeinflußt werden, werden diskutiert. Die Rißlängen und Rißtiefen werden mit Ultrasschallmethoden bestimmt. Die Grenzen der Identifizierung und der Größenbestimmung werden diskutiert.

La détection et le dimensionnement de fissures radiales, obtenues par des empreintes de Vickers dans un nitrure de silice, sont étudiés en utilisant des ondes de Rayleigh rayonnantes. La profondeur des fissures examinées varie entre 40 et 270 μm. La fréquence nominale des traducteurs focalisants utilisés est de 30 et 75 MHz. Les images C-scan compliquées par la présence de l'empreinte sont interprétées. La longueur et la profondeur des fissues sont mesurées par des méthodes ultrasonores. Les limites de détection et de dimensionnement sont discutées.

1 Introduction

Engineering ceramics, such as Si_3N_4, SiC and ZrO_2 show potential for use in structural applications where high mechanical and high thermal loading occur. However, due to their brittle nature, their mechanical properties show a wide variability and failure is generally caused by small defects such as microcracks, voids, inclusions and oversized grains[1–4] Amongst these defects surface-breaking cracks form an important category. The critical flaw size in ceramics varies between 50 and 500 μm.[5] Ideally the detection limit should be 10 μm.[6,7]

Ultrasonics is one of the most suitable non-destructive techniques for detection and characterisation of cracks. Methods, based upon the use of leaky Rayleigh waves, have often been applied to detect and characterise shallow surface-breaking cracks.[8–22] Leaky Rayleigh waves lend themselves better to the detection of surface-breaking cracks than the better known and more widely used bulk compression or shear waves, because their energy is contained in a region less than two wavelengths below the surface, making them very sensitive to the presence of surface defects. Two of the most widely used techniques are a pulse echo technique and acoustic microscopy.[8–22]

In acoustic microscopy[8–13] the interference phenomena between waves radiated by leaky Rayleigh waves propagating in all directions along the surface and the wave reflected specularly on the surface are exploited to obtain acoustic images. The

Journal of the European Ceramic Society 0955-2219/93/$6.00

frequencies used vary from 100 MHz up to some GHz. Scanning acoustic microscopy has been used extensively, and with success, to image surface defects.

In the pulse echo technique[14-22] the reflection of Rayleigh waves on surface-breaking defects is studied. The Rayleigh waves are propagating in one specific direction. Most of the attention until now has been directed towards signal analysis to detect and characterise the defects. For maximum detectability measurements should be made at a wavelength (λ_R) comparable to or smaller than the crack size.[16] A typical value for the wavelength in silicon nitride is 100 μm at 50 MHz, illustrating the need to use frequencies much higher than normally used in non-destructive testing.

Relatively little attention has been paid to image surface defects using this last technique. Jagnoux & Vincent[23] used it to image surface defects in metals. Clarke *et al.*[16] equipped their acoustic microscope with a special acoustic objective to eliminate the specular reflection. They imaged slot-like surface cracks in silicon nitride. The frequency used varied between 35 and 50 MHz.

The resolution obtained with acoustic microscopy is undoubtedly better but very high frequencies need to be used, limiting the penetration depth to some microns. Despite the lower resolution obtained with the pulse-echo technique it presents a number of non-negligible advantages:

- The use of lower frequencies in the pulse-echo technique means larger penetration depths, allowing one to obtain information on the crack depth. Different methods have been developed and used to measure the crack depth.[17-21]
- The pulse-echo technique is very sensitive to the presence of cracks which are orientated orthogonally with respect to their propagation direction. In acoustic microscopy there are no preferential directions. Furthermore, only a tiny disturbance (caused by the leaky Rayleigh waves) to a large output signal (due to the specular reflection) is measured.[16] So for frequencies of around 50 MHz the pulse-echo technique is more sensitive to the presence of the type of cracks mentioned than acoustic microscopy. Note, on the other hand, that cracks which are not orientated orthogonally with respect to the propagation direction of the leaky Rayleigh waves are not detected by the pulse-echo technique. For acoustic microscopy the orientation of the crack does not play a role.
- Rayleigh waves can propagate along curved surfaces, provided that the curvature is large with respect to the wavelength. So inspection *in situ* of components can be envisaged.[21] This is not the case for acoustic microscopy where only relatively small specimens can be investigated. Moreover the surface has to be flat and well polished.

The purpose of this publication is to show the possibilities of detecting, imaging and characterising surface-breaking cracks in a sintered reaction-bonded silicon nitride by the pulse-echo technique. Firstly, the main characteristics of the defects studied are given. Then the main properties of the leaky Rayleigh waves are recalled. Next the ultrasonic imaging system is described and examples of images are given and discussed in detail. Crack lengths, determined from the ultrasonic images, are compared with the real dimensions. Also crack depth measurements are presented. Finally, the influence of the used frequency on detection, imaging and sizing is discussed.

2 Experimental

2.1 Material and defects

The material used for the experiments was a sintered reaction-bonded silicon nitride (SRBSN). It contained Y_2O_3, Al_2O_3 and MgO as sintering additives.

The defects studied were radial cracks, resulting from Vickers indents. These are quite representative of natural surface-breaking cracks. Figure 1 shows a schematic diagram of the crack pattern, resulting from a Vickers indent in a brittle material.[24,25] It consists of two half-elliptical surface-breaking cracks, orientated parallel with the indent diagonals, and normally referred to as radial cracks. Furthermore, there are also the so-called lateral cracks spreading outwards from the deformation zone, beneath the indent surface.

The SRBSN test bar in which the indents were made was 20 mm long, 4·4 mm wide and 3·3 mm thick. Six indents were made on the polished surface (4·4 mm × 20 mm) of the bar as shown in Fig. 2.

Table 1 summarises the most interesting characteristics of each indent. The diagonal of the indent and the radial crack length were measured from scanning electron microscopy (SEM) micrographs.

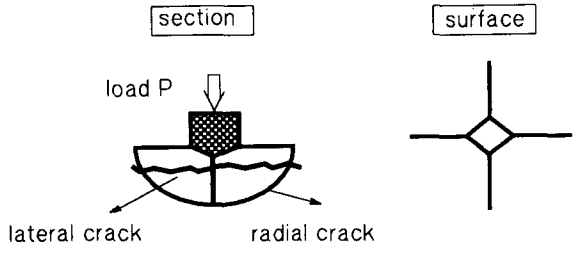

Fig. 1. Schematic representation of a crack pattern, resulting from a Vickers indent in a brittle material.

Table 1. Main characteristics of Vickers indents and corresponding radial cracks

Vickers load (N)	*Indent diagonal (μm)*	*Radial crack length (μm)*	*Maximum indent depth[a] (μm)*	*Maximum radial crack depth[a] (μm)*
300	200	540	40	270
200	160	400	32	200
100	110	260	22	130
50	80	150	16	75
30	60	110	12	55
20	50	80	10	40

[a] Calculated.

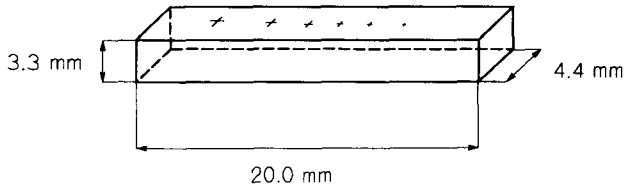

Fig. 2. Test bar of SRBSN used for the experiments.

The indent depth was calculated using the known geometry of the Vickers diamond. To a first approximation, it can be assumed that the maximum depth of the radial crack is half its length at the surface.[24,25]

Figure 3 shows a SEM image of indent 3. The radial crack, imaged with leaky Rayleigh waves (see Fig. 7 and Fig. 11), is indicated by arrows in Fig. 3.

2.2 Ultrasonic methods

2.2.1 Properties of leaky Rayleigh waves

When an ultrasonic beam impinges at an angle of incidence near the Rayleigh angle, onto the surface of a material immersed in a liquid, leaky Rayleigh waves are generated in the material. The Rayleigh angle, θ_R, is given by Snell's law:

$$\theta_R = \text{asin}\left(\frac{C_W}{C_R}\right)$$

with C_W (m/s) the propagation velocity of the longitudinal waves in the liquid and C_R (m/s) that of the leaky Rayleigh waves in the solid. Leaky Rayleigh waves have the following characteristics[23]:

- They propagate in the solid parallel to the solid–liquid interface with a velocity slightly lower than that of the shear waves in the solid.
- Their penetration depth is about one wavelength.
- They are attenuated as they propagate in the solid. This attenuation is mainly due to radiation of an energy flux back into the water at the Rayleigh angle.

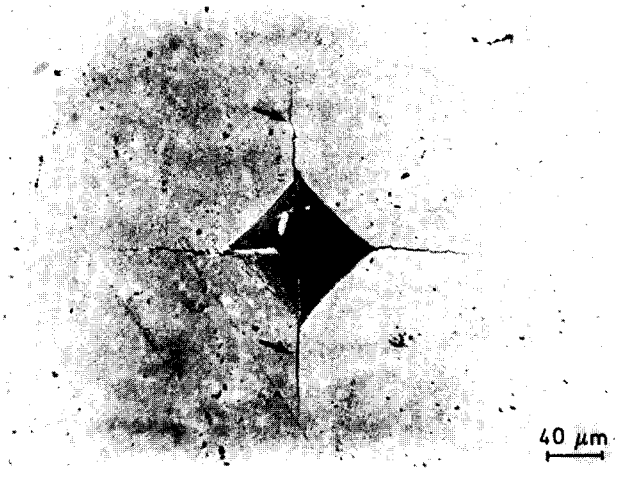

Fig. 3. SEM image of indent 3.

2.2.2 Ultrasonic imaging

Figure 4 shows the basic pulse-echo configuration used to generate and detect leaky Rayleigh waves. The transmitter probe, which in echo-mode also acts as receiver, is inclined at an angle close to the Rayleigh angle. An electrical pulse is applied to the probe, which produces a short ultrasonic pulse. This propagates through the water into the specimen. Leaky Rayleigh waves are generated which propagate in the specimen along the surface. When they

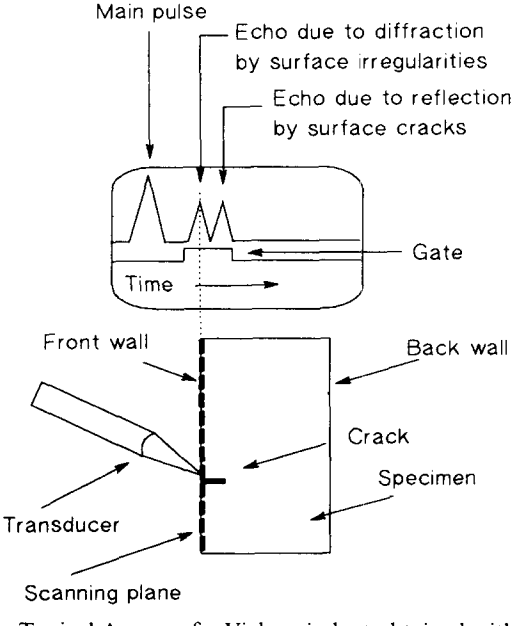

Fig. 4. Typical A-scan of a Vickers indent obtained with leaky Rayleigh waves.

are reflected by a surface-breaking crack part of the energy radiated back into the water returns to the probe. An electrical signal is produced which is delayed with respect to the emitting pulse. The representation as a function of time of the latter signal and its echo on a defect is called an A-scan. Figure 4 shows schematically an A-scan of a Vickers indent obtained with a probe inclined at the Rayleigh angle.

Note that in the A-scan two echoes are present at the surface. Besides the echo due to reflection of the leaky Rayleigh waves by the radial crack there is also an echo due to diffraction in water of the incident beam on surface irregularities (such as the indent). This latter echo arrives somewhat before the former one.

A C-scan image is obtained as follows. A part of the A-scan is selected by an adjustable time gate. In this case the gate intercepts the echo due to the leaky Rayleigh waves and the echo diffracted from the indent. The probe is scanned mechanically step-by-step in a regular raster over the surface of the specimen. The movement of the probe is parallel with the surface of the specimen. A parameter of the selected echo, in most cases the amplitude, is acquired for each position of the probe. The two-dimensional representation of the variation of this parameter as a function of probe position is a C-scan.

2.2.3 Crack length and crack depth measurement

The 6 dB amplitude drop technique[26] was used to estimate the crack length. The technique consists of first positioning the probe to obtain the peak amplitude of the echo reflected from the radial crack. The crack length is obtained by moving the probe along the crack until the amplitude has been reduced by a nominal amount of 6 dB.

An estimate of the crack depth can be obtained by measuring the peak amplitude A of the echo of the leaky Rayleigh waves on the crack. For short wavelength scattering, when both the crack radius $a \gg \lambda_R$ and the focal spot size of the beam are much larger than a, the amplitude A should be independent of a, whereas for long wavelength scattering when $a \ll \lambda_R$, A should be proportional to a^3.[21,22] For the transition zone, when a is comparable to λ_R or the focal spot size, no analytical expression is as yet known.

Ultrasonic spectroscopy has also been used by a number of authors to estimate crack depth and crack length.[17,19,20] Resonance phenomena, which are related to the crack depth and the crack length, may indeed be observed in the frequency spectrum of the echo of the reflected Rayleigh waves.

2.2.4 Ultrasonic equipment

Figure 5 shows a schematic overview of the equipment used. The pulser–receiver used was a Panametrics 5052 PRX with a band width of 75 MHz for the 30 MHz probe and a Panametrics 5601A with a band width of 150 MHz for the 75 MHz probe. The digital oscilloscope used was a LeCroy 9450 having a sampling rate of 400 MS/s and a band width of 350 MHz. This programmable oscilloscope allows the amplitude of the signal of interest to be acquired. After acquisition the amplitude information is transmitted via an IEEE-488 interface to a microcomputer (HP 300). The step-by-step motors (minimum step 10 μm), which in this case move the specimen instead of the probe, are also driven by the microcomputer through the same interface.

Two focusing polyvinylidene fluoride (PVDF) probes were used. PVDF is an organic material with interesting piezo-electric properties. Its main advan-

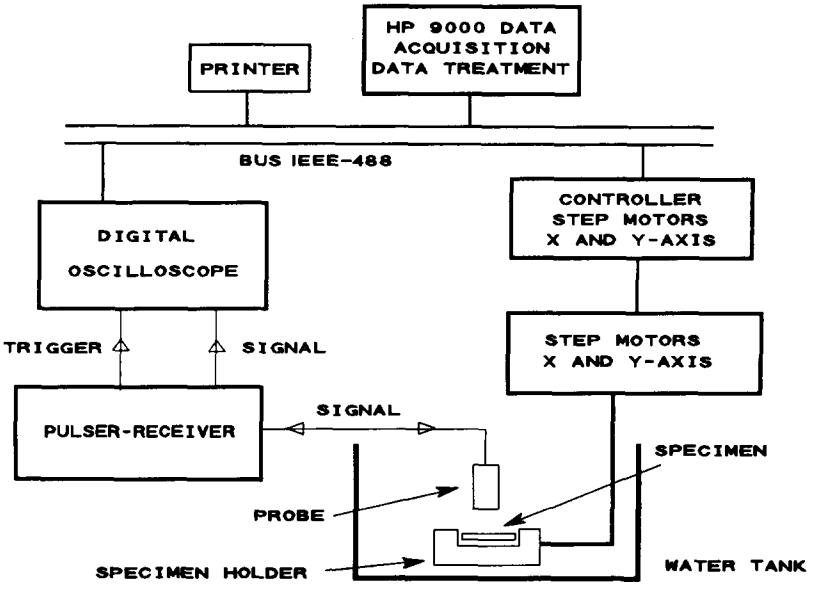

Fig. 5. Overview of ultrasonic equipment used.

Table 2. Main characteristics of focusing probes used, their corresponding beam and signal due to the leaky Rayleigh waves

	Characteristic	*Probe 1*	*Probe 2*
Probe	Nominal frequency (MHz)	30	75
	Diameter (mm)	3·1	3·1
	Nominal focal distance (mm)	20	12·7
	Effective focal distance (mm)	17·5	12·5
Signal	Central frequency (MHz)	28	60
	Band width (%)	90	15
Beam	Focal spot size[a] (μm)	280	100

[a] Calculated.

tage, however, is its film character which can be produced at a thickness for which the more classical ceramic materials would be extremely fragile.[26] Focalisation is hence obtained directly by depositing it on a segment of a sphere. With classical piezoelectric materials a delay line has to be used to focus the beam. Internal reflections within the delay line cause a lot of noise, diminishing the sensitivity.

The main parameters of the two focusing PVDF probes are given in Table 2. The nominal frequency of the probes are 30 and 75 MHz respectively. As these probes have a large band width, the central frequency of the spectrum of the echo also depends on the exact configuration of the equipment used and the attenuation in water. The spectra of the signals due to the leaky Rayleigh waves are centred at 28 MHz and 60 MHz, with a band width of 90% and 15% respectively. In order to obtain the central frequency of 60 MHz for the 75 MHz probe it was necessary to use a very short coaxial cable (15 cm) and an analogue high-pass filter. That is why the band width of the 75 MHz probe is relatively small. The focal distance of the probe corresponds to the distance between probe and specimen for which the amplitude of the front wall echo, obtained in normal incidence, becomes a maximum. For the 30 MHz probe the measured focal distance was found to be 10% lower than the nominal one. The focal spot size d was calculated as follows:[26]

$$d = \left(\frac{C_w \cdot F}{f_c \cdot D}\right)$$

with F the focal distance of the probe, f_c the central frequency and D the diameter of the probe.

3 Results

3.1 Detection and imaging

Figure 6 shows two C-scans, obtained with the 30 MHz and the 75 MHz probe respectively. The

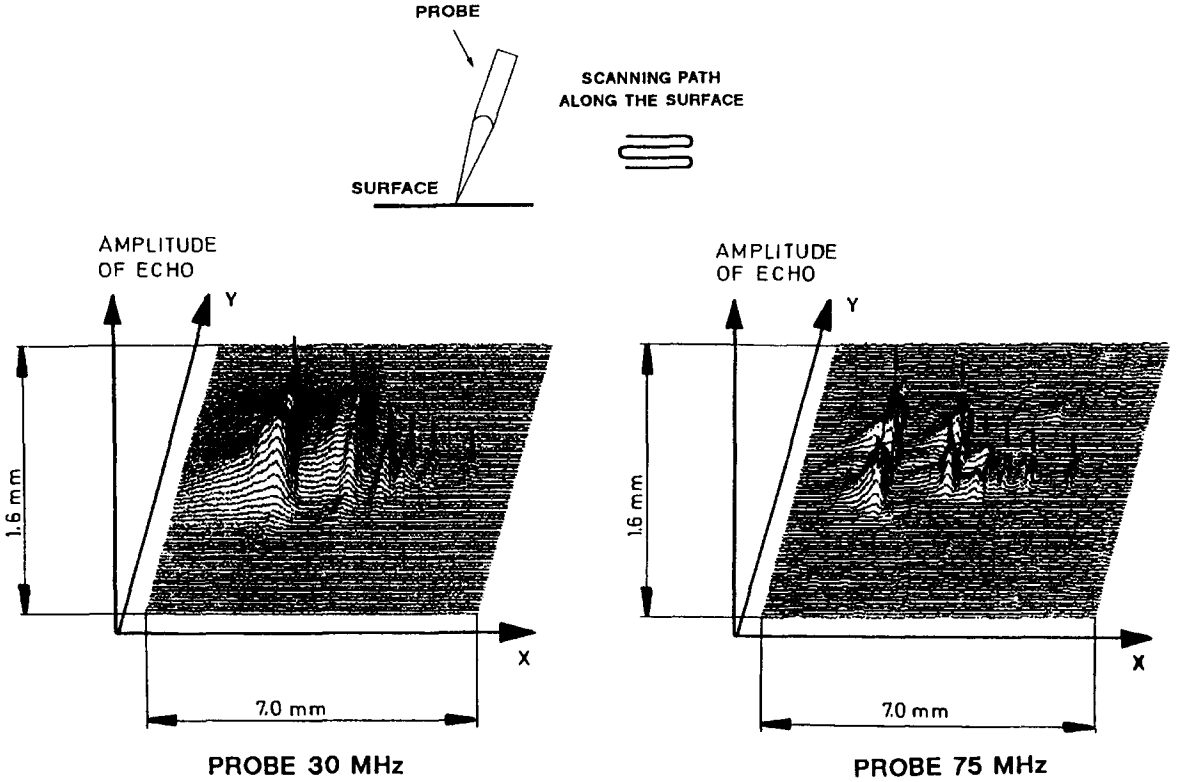

Fig. 6. C-Scans of area containing all six indents, obtained with the 30 MHz and the 75 MHz probe respectively (step 20 μm).

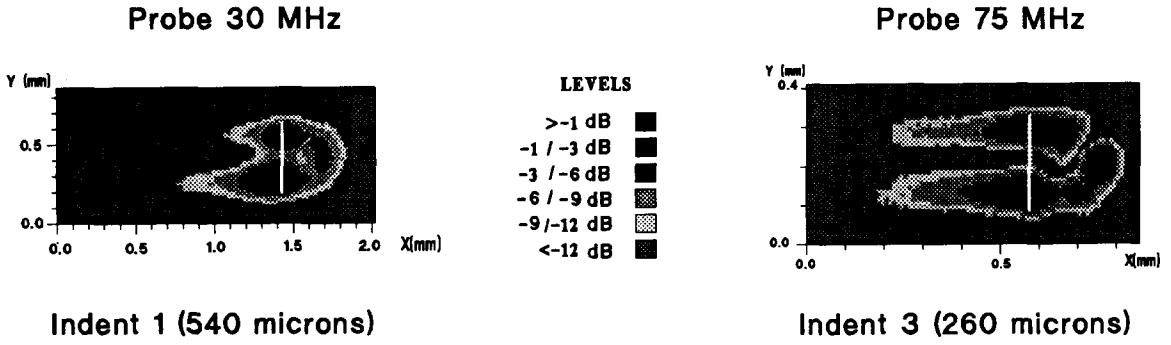

Fig. 7. C-Scan of indent 1 (radial crack length 540 μm) obtained with the 30 MHz probe and of indent 3 (radial crack length 260 μm) obtained with the 75 MHz probe.

arrows indicate the peaks corresponding to the different indents. All six indents were detected by both probes. Comparing the two images indicates that the 75 MHz probe has a higher sensitivity than the 30 MHz probe. The noise visible in the images varies in an arbitrary way from one scanning line to the next. As the scanning step is much smaller than the focal spot size, this suggests that the nature of the noise is electronic.

Figure 7 shows two C-scans, the first of indent 1 (radial crack length 540 μm) and the second of indent 3 (radial crack length 260 μm) obtained with the 30 MHz probe and the 75 MHz probe respectively. The grey levels are graduated in dB, the 0 dB level corresponding to the maximum amplitude of the echo due to the leaky Rayleigh waves. These images, showing three maxima, are typical of the larger indents. The white straight lines indicate the crack lengths determined with the 6 dB amplitude drop technique.

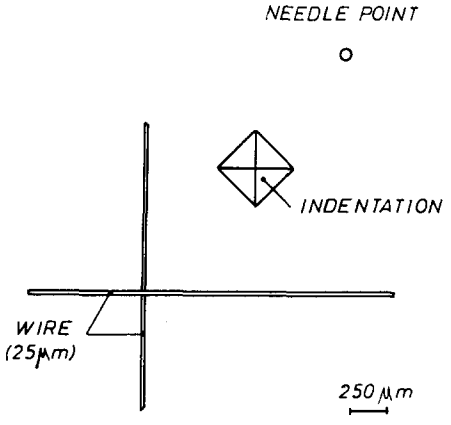

Fig. 8a. Position of reference reflectors with respect to Vickers indent.

The exact origin of these three maxima has been studied by putting reference reflectors on the surface near the largest indent and recording the corresponding C-scan of the surface. Figure 8a shows the position of two 25 μm diameter wires (at 90° to each other) and a needle with respect to the Vickers indent. The needle is used as an additional reference point. Figure 8b represents the corresponding C-scan, obtained with the 30 MHz probe. In this image it is easy to recognise the reflection on the wire, which is orientated orthogonally with respect to the beam axis. A significant drop in reflection occurs at the intersection with the other wire, which is orientated parallel to the projection of the beam axis on the surface. Diffraction by the point of the needle

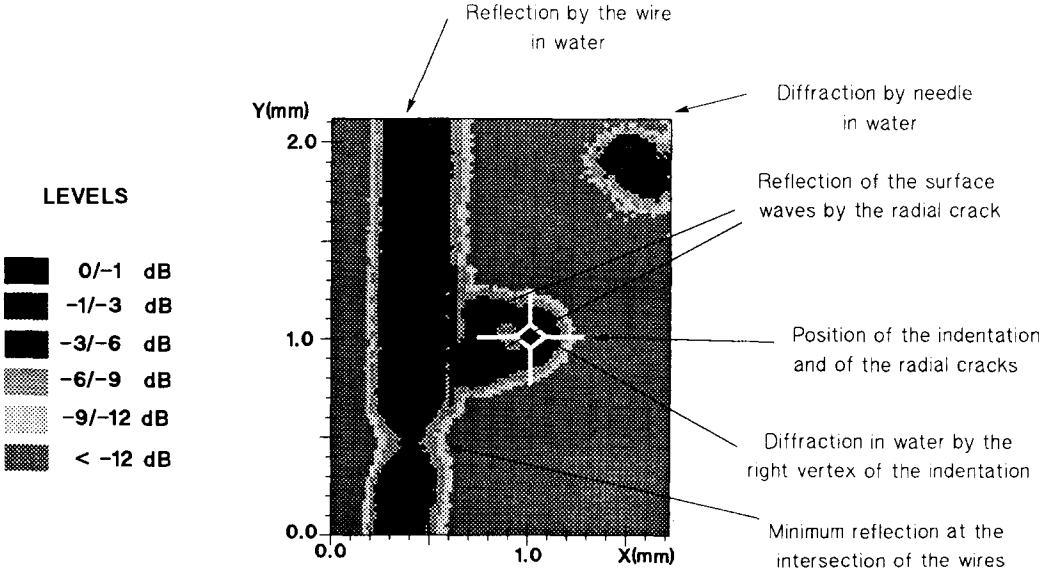

Fig. 8b. C-Scan of surface with reference reflectors.

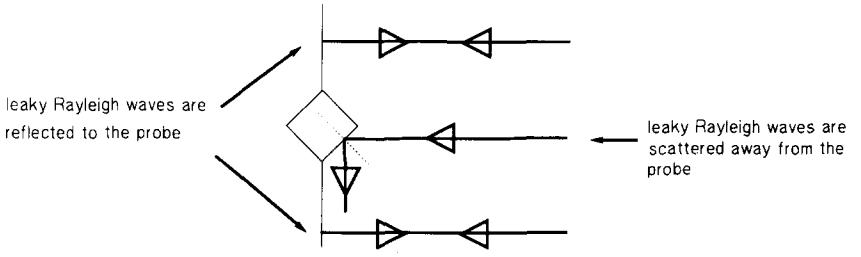

Fig. 9. Scattering of the leaky Rayleigh waves by the indent.

gives rise to the maximum in the upper right corner of the C-scan.

Three maxima due to the Vickers indent are clearly visible. The exact position of the indent and the radial cracks with respect to the reference reflectors, measured using an optical microscope, is also given in Fig. 8b. The maximum on the right is due to diffraction in water of the incident beam by the right vertex of the indent. The two other maxima, disposed symmetrically with respect to the indent, are due to reflection of the leaky Rayleigh waves by the radial crack, which is orientated perpendicular to their propagation direction. This reflection is characterised by three features:

- Two maxima are observed whereas only one would be expected (see also Fig. 7).
- The maximum reflection occurs when the beam hits the surface of the specimen some distance ahead of the crack.
- Elongated shape of the two maxima due to reflection of the leaky Rayleigh waves (see also Fig. 7).

In the central zone of the radial crack, where the indent is present, the leaky Rayleigh waves are scattered. As the penetration depth is one wavelength, λ_R, this causes an important decrease of reflection, as shown in Fig. 9. The central part of the crack is hence masked by the indent so that the leaky Rayleigh waves are only reflected by the extremities of the radial crack, explaining the presence of the two maxima.

Maximum reflection/diffraction is generally obtained when the ultrasonic beam hits the reflector itself. In the case of the leaky Rayleigh waves, however, the maximum reflection occurs when the beam hits the surface some distance ahead of the crack.

This can be explained in a qualitative way as follows. Only the leaky Rayleigh waves which are generated ahead of the crack are reflected, as shown in Fig. 10. If the beam hits the crack, only a part of the generated leaky Rayleigh can be reflected, whereas when the beam hits the surface some distance ahead of the crack, more leaky Rayleigh waves are reflected. The exact position of the probe where maximum reflection occurs depends also on the attenuation of the leaky Rayleigh waves. In the case of Fig. 8 the shift of the maximum reflection with respect to the position of the crack is about 200 μm.

The reflection of the leaky Rayleigh waves by the extremities of the radial crack gives rise to an elongated spot in the C-scan (see e.g. C-scans in Fig.

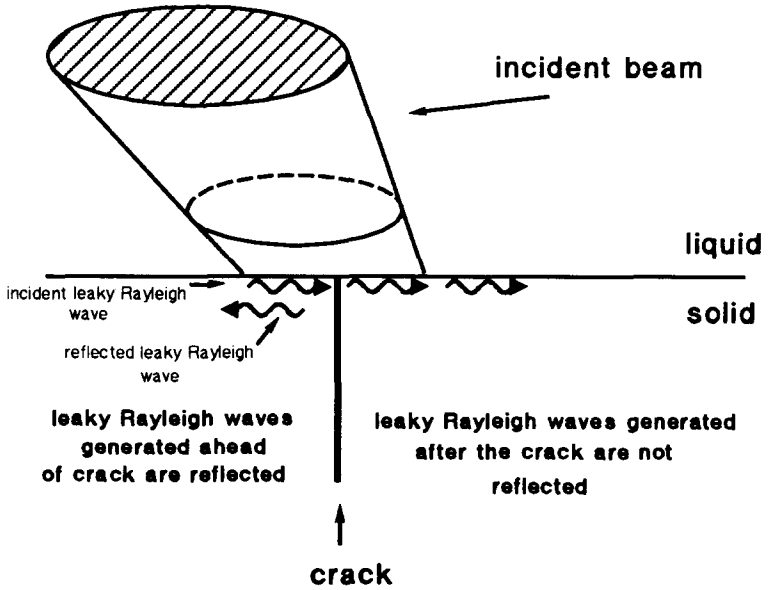

Fig. 10. Schematic diagram to explain the observed shift in maximum reflection.

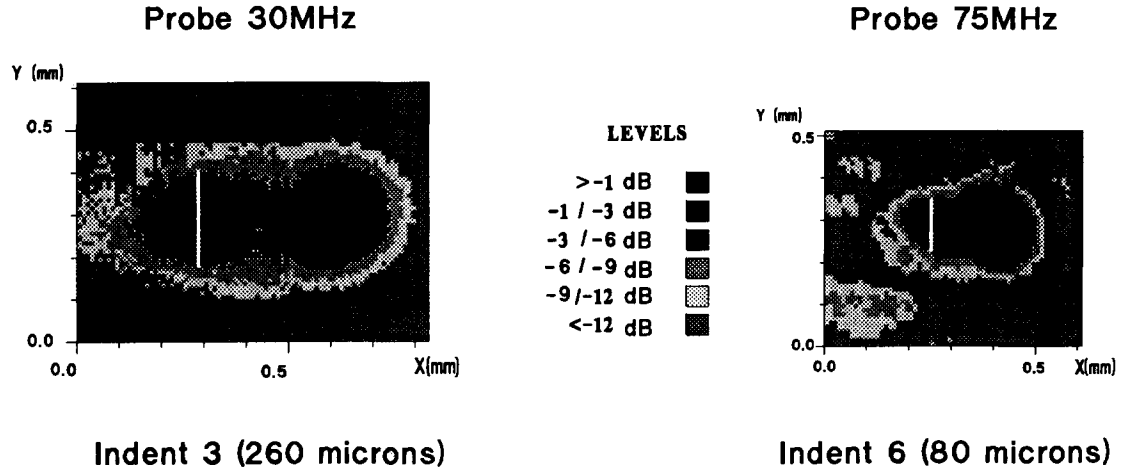

Fig. 11. C-Scan of indent 3 (radial crack length 260 μm) and of indent 6 (radial crack length 80 μm) obtained with the 30 MHz probe and the 75 MHz probe respectively.

7). This can be attributed to the fact that the attenuation of the reflected leaky Rayleigh waves is such that even after a travelling path of several tenths of millimetres they still can be detected. Note that the width of the time gate has to be large enough to detect them at these distances.

Figure 11 shows two C-scans, one of indent 3 (radial crack length 260 μm) and one of indent 6 (radial crack length 80 μm), obtained with the 30 MHz probe and the 75 MHz probe respectively. These two images, showing only two maxima, are typical of the C-scans obtained from the smaller indents. The maximum on the right is again due to diffraction in water by the right vertex of the indent, whereas the maximum on the left is due to reflection of the leaky Rayleigh waves by the radial crack. Only one maximum due to the leaky Rayleigh waves is now detected, as the focal spot size was too large to distinguish the central part of the crack masked by the indent. Note that indent 3 (radial crack length 260 μm) is the limiting case. With the 30 MHz probe only one maximum is detected (see Fig. 11), whereas with the 75 MHz probe two maxima are detected (see Fig. 7), showing the better resolving power of the 75 MHz probe. Indeed, the focal spot size of the beam of the 30 MHz probe is 280 μm, whereas that of the 75 MHz probe is 100 μm.

3.2 Crack length measurement

The vertical white straight lines on the C-scans (see Figs 7 and 11) represent the radial crack length determined with the 6 dB amplitude drop method. The results obtained are compared in Table 3 with the real crack lengths measured from SEM micrographs. The crack lengths given refer to one radial crack.

The leaky Rayleigh waves, obtained with the 30 MHz probe, allow measurement of the radial cracks lengths of 540 μm, 400 μm and 260 μm with an error of less than 20%. The radial crack of 150 μm is oversized by a factor of 2, whereas the two smallest cracks of 110 and 80 μm are oversized by a factor 4.

Similarly, for the 75 MHz probe the 540 μm, 400 μm, 260 μm and 150 μm radial crack lengths were measured with an error less than 20%. The error for the crack of 110 μm is about 20%, whereas for the smallest crack of 80 μm the error is about 50%. The results can be considered to be satisfactory. It is clear that the method of the 6 dB amplitude drop is not valid when the focal spot size is larger than the radial crack length to be measured.

3.3 Crack depth measurement

Figure 12 shows the amplitude A received at the 30 and 75 MHz probe as a function of crack depth a.

Table 3. Radial crack length measurements by the 6 dB amplitude drop method

Crack	*Crack length measured by SEM (μm)*	*Crack length determined using 30 MHz leaky Rayleigh waves (μm)*	*Crack length determined using 60 MHz leaky Rayleigh waves (μm)*
1	540	470	530
2	400	400	400
3	260	280	270
4	150	280	180
5	110	400	140
6	80	320	130

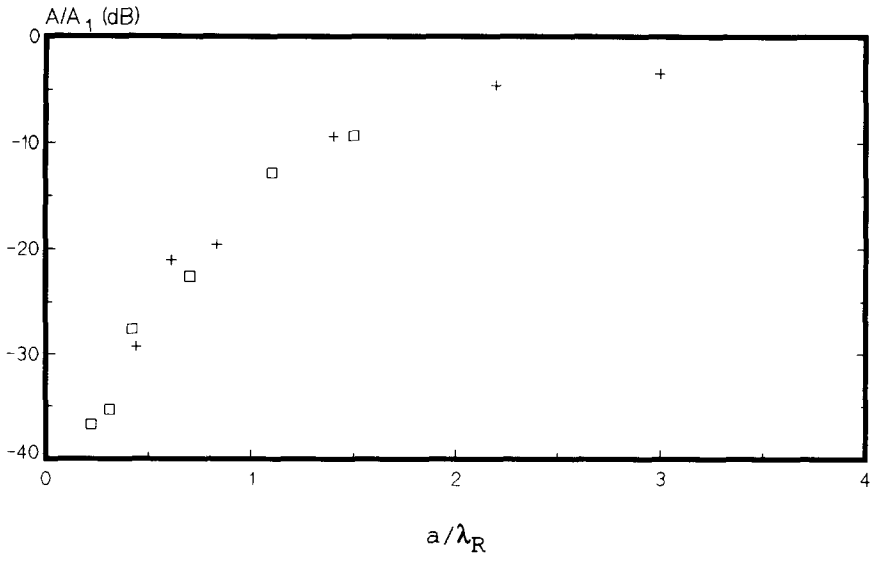

Fig. 12. Normalised maximum amplitude of the crack echo as a function of normalised crack depth.

The amplitude A is normalised with respect to the amplitude $A1$ received from a 90° corner and is expressed in dB. The crack depth is normalised with respect to the Rayleigh wavelength λ_R. One can distinguish quite easily the two regions, which are predicted by theory. Firstly, there is the rapid increase of the amplitude A with crack size for $a < \lambda_R$. When a becomes larger than λ_R saturation occurs. The results correspond well with those obtained by Fahr & Sturrock,[19] obtained on cracks induced by Knoop indentations in a hot-pressed silicon nitride.

Ultrasonic spectroscopy was unsuccessful, most probably because the presence of the indent influenced in a non-negligible way the frequency spectra.

4 Discussion

Thanks to the use of reference reflectors it was possible to give a satisfactory explanation of the C-scans recorded. It has been shown that the maximum reflection of the leaky Rayleigh waves by the radial crack occurs when the beam hits the surface of the specimen some distance ahead of the crack. This is in agreement with the findings of a model describing in a quantitative way the ultrasonic response of a surface-breaking crack, irradiated by focused leaky Rayleigh waves.[27] Furthermore, the non-negligible influence of the indent on the image has been explained.

The 30 MHz probe allowed the authors to distinguish between the two extremities of a radial crack, each about 120 μm long and separated by an indent 160 μm wide (total radial crack length 400 μm). The 75 MHz probe has a much better resolving power. It allowed the authors to distinguish between the two extremities of a radial crack, each about 75 μm long and separated by an indent of 110 μm wide (total radial crack length 260 μm). The smallest radial crack detected was 80 μm long and has a maximum depth of 40 μm. Note that 10% of its surface is masked by the indent. Lateral cracks may mask a larger part of the radial crack. The signal/electronic noise ratio of the 75 MHz probe was also significantly better, especially for the smaller cracks. This can be attributed on the one hand to the smaller focal spot size and on the other to the smaller penetration depth of the leaky Rayleigh waves at higher frequencies.

The sizing limit of the crack length, estimated with the amplitude drop technique, depends mainly on the focal spot size of the incident beam. In this respect the 75 MHz probe is again superior to the 30 MHz probe, as the focal spot size diminishes from 280 μm to 100 μm.

The results obtained at 30 MHz with respect to imaging and crack length estimation are in good agreement with those obtained previously[28] on a reaction-bonded silicon nitride (RBSN), containing slightly larger radial cracks (100–600 μm in comparison to 80–540 μm).

A rough estimate of the crack depth a can be obtained by measuring the maximum amplitude of the echo of the leaky Rayleigh waves. At 30 MHz the ratio a/λ_R varies roughly between 0·2 and 1·5, whereas at 60 MHz it varies between 0·4 and 3. Consequently in the given conditions saturation occurs with increasing crack size for the 75 MHz probe, whereas for the 30 MHz probe it is less pronounced. For the examined range of crack depths the 30 MHz probe is more suitable for estimating crack depth.

If a surface-breaking crack is close to a surface irregularity, as is the case with the radial rack and the indent, it is important to distinguish the echo on the surface irregularity from that on the crack. The first echo arrives somewhat before the second one. If,

Table 4. Ratio of amplitudes of echo on radial crack with respect to that on indent

Indent	*Indentation depth* (μm)	*Crack depth a* (μm)	*Ratio of amplitudes at 30 MHz*	*Ratio of amplitudes at 60 MHz*
1	40	270	1·5	1·9
2	32	200	1·0	1·9
3	22	130	1·0	1·0
4	16	75	0·9	0·4
5	12	55	0·6	0·4
6	10	40	1·0	0·2

however, the echo on the crack is much smaller than that on a surface irregularity, the former echo may get masked by the tail of the latter echo. This is illustrated in Table 4, which shows how the ratio between the amplitude of the echo on the radial crack and on the indent varies with crack and indent depth. For the 30 MHz probe this ratio varies between 1·5 for the largest indent and 0·6 for indent 5, whereas for the 75 MHz probe this ratio diminishes from 1·9 to 0·2 with decreasing crack and indent depth. This means that for the smallest indentation the amplitude of the echo on the crack (depth 40 μm) is five times smaller than that on the indent (depth 10 μm) at 75 MHz, whereas at 30 MHz both echoes are about equal in amplitude. This implies further that for a surface roughness of 10 μm the crack of 40 μm will certainly not be detectable at 75 MHz, whereas at 30 MHz a possibility for detection may exist. This illustrates that when working at higher frequencies good surface conditions are required.

5 Conclusions

The authors have shown the possibilities of a pulse-echo technique, based on the use of focused leaky Rayleigh waves to image and characterise shallow surface-breaking cracks, whose depth varied between 40 and 270 μm. The obtained C-scan images could be interpreted satisfactorily. The best results with respect to imaging and crack length measurement were obtained with the 75 MHz probe, whereas for crack depth estimation the best results were obtained with the 30 MHz probe.

Increasing the frequency may yet improve the performance of the technique with respect to imaging and crack length estimation. This would require very good surface conditions as the signals due to surface irregularities increase significantly with frequency. Thus an interesting point for further study is the optimisation of the design of the probe in order to increase the ratio of the signals due to surface cracks with respect to those due to surface irregularities. For this purpose, the model as described in Ref. 27 will be very useful.

Acknowledgements

The authors wish to thank Dr E. Bullock from JRC Petten for providing the specimen with the indents and F. Gandrey for performing the ultrasonic crack depth measurements.

References

1. Thümmler, F., Engineering ceramics: state of the art. *J. Eur. Ceram. Soc.*, **6** (1990) 139–51.
2. Davidge, R., *Mechanical Behaviour of Ceramics.* Cambridge University Press, Oxford, UK, 1979.
3. Lemaitre, P., Gilissen, R., Smolders, J. & Koenen, J., Relationships between Fabrication, microstructure and mechanical properties of injection moulded Si_3N_4. In *Proceedings of the 1st Eur. Ceram. Soc. Conf.*, ed. G. de With, R. Terpstra & R. Metselaar. Elsevier Applied Science, London, 1989, pp. 1.270–5.
4. Roth, D. J., Flaw characterisation in structural ceramics using scanning laser acoustic microscopy. NASA N 88-22415, Cleveland, Ohio, USA, 1988.
5. Evans, A. G., Aspects of the reliability of ceramics. In *Defect Properties and Processing of High-Technology Non-Metallic Materials*, ed. J. H. Crawford, Jr, Y. Chen & W. A. Sibley. North-Holland, New York, 1984, pp. 63–80.
6. Khandelwal, P. K., Non-destructive evaluation of structural ceramics by photoacoustic microscopy: Final report. General Motors, NASA N 88-16868, Cleveland, Ohio, USA, 1988.
7. Goebbels, K. Reiter, H., Arnold, W. & Hirsekorn, S., Ein Konzept zur Qualitätssicherung von Bauteilen der Keramik-Gasturbine durch Zerstörungsfreie Prüfung. Berlin, FRG, BMFT-FB-T 85-094, 1985.
8. Briggs, A., *An Introduction to Scanning Acoustic Microscopy.* Oxford University Press, Royal Microscopical Society, Oxford, UK, 1985.
9. Yamanika, K. & Enomoto, Y., Detection and characterization of surface cracks with scanning acoustic microscope. *J. Appl. Phys.*, **53** (1982) 846–50.
10. Nongaillard, B., Logette, P., Rouvaen, J., Saisse, J. & Fevrier, H., Acoustic microscopy: a tool for non-destructive evaluation of ceramics. *NDT International*, **19** (1986) 77–82.
11. Fatkin, D., Scruby, C. & Briggs, G., Review: acoustic microscopy of low-ductility materials. *J. Mat. Sci.*, **24** (1989) 23–40.
12. Parent, P., Chou, C-H. & Khury-Yakub, B., Ball-bearing inspection with an acoustic microscope. In *IEEE Ultrasonics Symposium*, IEEE, New York, USA, 1988, pp. 1111–13.
13. Scruby, C., Lawrence, C., Fatkin, D., Briggs, G., Dunhill, A., Gee, A. & Chao, C.-L., Non-destructive testing of ceramics by acoustic microscopy. *Brit. Ceram. Trans. J.*, **88** (1989) 127–32.
14. Khury-Yakub, B., Kino, G., Liang, K., Ten, J., Chou, C-H., Evans, A. & Marshall, D., Non-destructive evaluation of ceramics. In *Review of Progress in Quantitative*

NDE.Thompson, D. O. and Chimenti, D. E. Plenum Press, New York, 1982, pp. 601–5.
15. Khury-Yakub, B., Shui, Y., Kino, G., Marshall, D. & Evans, A., Measurement of surface machining damage in ceramics. In *Review of Progress in Quantitative NDE*. Thompson, D. O. and Chimenti, D. E. Plenum Press, New York, 1983, pp. 229–37.
16. Clarke, L., Chou, C-H., Khuri-Yakub, B. & Marshall, D., Acoustic evaluation of grinding damage to ceramic materials. In *Proceedings of the Second International Symposium on Ceramic Materials and Components for Engines*, ed. W. Bunk & H. Hausner. DKG, Lübeck, Travemunde, FRG, 1986, pp. 789–97.
17. Bond, L. & Saffari, N., Crack characterization in turbine disks. In *Review of Progress in Quantitative NDE*. Thompson, D. O. and Chimenti, D. E. Plenum Press, New York, 1983, pp. 251–61.
18. Fahr, A., Johar, S., Murthy, M. & Sturrock, W., Surface acoustic wave studies of surface cracks in ceramics. In *Review of Progress in Quantitative NDE*. Thompson, D. O. and Chimenti, D. E. Plenum Press, New York, 1983, pp. 239–49.
19. Fahr, A. & Sturrock, W., Detection and characterization of surface cracks using leaky Rayleigh waves. In *Review of Progress in Quantitative NDE*, Vol. 4A. Thompson, D. O. and Chimenti, D. E. Plenum Press, New York, 1985, pp. 559–68.
20. Domarkas, V., Khuri-Yakub, B. & Kino, G., Length and depth resonances of surface cracks and their use for crack size estimation. *Appl. Phys. Lett.*, **33** (1978) 557–9.
21. Khuri-Yakub, B., Kino, G. & Evans, A., Acoustic surface wave measurements of surface cracks in ceramics. *J. Am. Ceram. Soc.*, **63** (1980) 65–7.
22. Auld, B., General electromechanical reciprocity relations applied to the calculation of elastic wave scattering coefficients. *Wave Motion*, **1** (1979) 3–10.
23. Jagnoux, P. & Vincent, A., Ultrasonic imaging by Leaky Rayleigh waves. *NDT International*, **22** (1989) 339–46.
24. Anstis, G. R., Chantikul, P., Lawn, B. R. & Marshall, D. B., A critical evaluation of indentation techniques for measuring fracture toughness: I. Direct crack measurement. *J. Am. Ceram. Soc.*, **64** (1981) 533–8.
25. Lawn, B. R., Evans, A. G. & Marshall, D. B., Indentation damage in ceramics: The median/radial crack system. *J. Am. Ceram. Soc.*, **63** (1980) 574–81.
26. Krautkrämer, J. & Krautkrämer, H., *Ultrasonic Testing of Materials*. Springer-Verlag, New York, Heidelberg, Berlin, 1990.
27. Lakestani, F. & Lemaitre, P., Detection of sizing of surface-breaking cracks by focalized surface waves: Experimental results and theoretical modelling. In *Proceedings Progress in metals and new materials investigation methods, 8th International Symposium—Cercle d'études des métaux—Saint Etienne*, École nationale supérieure des mines, Saint-Etienne, France, 20–21 November 1991.
28. Lemaitre, P., Lakestani, F., Denis, R. & Gandrey, F., Non-destructive ultrasonic characterisation of cracks in reaction-bonded silicon nitride (RBSN). In *Proceedings of the European Ceramic Society Second Conference*, Augsburg, FRG, 11–14 September 1991.